Available online at www.sciencedirect.com
SCIENCE DIRECT
Journal of Power Sources 155 (2006) 231–238
JOURNAL OF POWER SOURCES
www.elsevier.com/locate/jpowsour

A study of carbon formation and prevention in hydrocarbon-fueled SOFC

T. Kim [a], G. Liu [a], M. Boaro [a], S.-I. Lee [a], J.M. Vohs [a], R.J. Gorte [a,*], O.H. Al-Madhi [b], B.O. Dabbousi [b,1]

[a] *Department of Chemical and Biomolecular Engineering, University of Pennsylvania, 311 Towne Building, 220 South 33rd Street, Philadelphia, PA 19104, USA*
[b] *Saudi Aramco, Research and Development Center, Dhahran, Saudi Arabia 31311*

Received 31 March 2005; received in revised form 27 April 2005; accepted 2 May 2005
Available online 14 June 2005

Abstract

The formation and removal of the carbonaceous deposits formed by *n*-butane and liquid hydrocarbons, such as *n*-decane and proprietary light and heavy naphthas, between 973 and 1073 K on YSZ and ceria–YSZ, has been studied to determine conditions for stable operation of direct-utilization SOFC. First, it is shown that deactivation of SOFC with Cu–ceria–YSZ anodes operating on undiluted *n*-decane, a mixture of 80% *n*-decane and 20% toluene, or light naphtha at temperatures above 973 K is due to filling of the pores with polyaromatic compounds formed by gas-phase, free-radical reactions. Formation of these compounds occurs at a negligible rate below 973 K but increases rapidly above this temperature. The rate of formation also depends on the residence time of the fuel in the anode compartment. Because steam does not participate in the gas-phase reactions, carbonaceous deposits could form even at a H_2O:C ratio of 1.5, a value greater than the stability threshold predicted by thermodynamic calculations. Temperature programmed oxidation (TPO) measurements with 20% H_2O in He demonstrated that carbon deposits formed in pure YSZ were unreactive below 1073 K, while deposits formed on ceria-YSZ could be removed at temperatures as low as 923 K. Based on these results, we discuss strategies for avoiding carbon formation during the operation of direct-utilization anodes on oil-based liquid fuels.

Keywords: Solid oxide full cell; Hydrocarbon fuels; Carbon formation; Gas-phase pyrolysis; Ceria; Yttria-stabilized zirconia

1. Introduction

The formation of "carbon" is a serious problem with many processes that involve hydrocarbons at high temperatures, including solid oxide fuel cells (SOFC). Because direct utilization of hydrocarbons is theoretically possible in SOFC [1], the primary reason to reform hydrocarbons to syngas, a mixture of CO and H_2, before sending them to the anode is that feeding the hydrocarbons directly would result in carbon formation, which would in turn quickly deactivate the cells. To achieve stable operation, it is often assumed that one must determine the thermodynamic regime where carbon is predicted to be unstable and to operate the cell in that regime [2–5].

Unfortunately, the thermodynamic analysis is not appropriate in this case because it assumes that the rates of the forward reaction (carbon deposition) and the reverse reaction (carbon removal) are rapid enough to establish equilibrium, an assumption that cannot be justified. For example, hydrocarbons are stable towards decomposition for geologically long times at low temperatures, even though reaction to carbon may be thermodynamically predicted. On the other hand, there are many examples where carbon does form under conditions where it is predicted to be thermodynamically unstable. For example, based on the calculations of Sasaki and Teraoka, carbon is thermodynamically unstable towards reaction to CO and CO_2 for essentially all hydrocarbon fuels

* Corresponding author. Tel.: +1 215 898 4439; fax: +1 215 573 2093.
E-mail addresses: gorte@seas.upenn.edu (R.J. Gorte), bashir.dabbousi@aramco.com (B.O. Dabbousi).
[1] Tel.: 9663 872 5120; fax: 9663 872 5208.

0378-7753/$ – see front matter © 2005 Elsevier B.V. All rights reserved.
doi:10.1016/j.jpowsour.2005.05.001

at 773 K when there is a H_2O:C ratio of 1.8 or greater [4]. However, it has been shown that carbon formation will occur at this temperature on Ni catalysts at H_2O:C ratios greater than 3.0 following the addition of even a few percent of olefins to methane [6]. Other studies have shown that conditions under which carbon deposits form on Ni and Co catalysts depend strongly on the metal particle size, a result that cannot be explained by thermodynamics [7].

To understand when carbon will form, it is important to understand the reactions that deposit and remove carbon. At least two mechanisms are known to exist at high temperatures for carbon deposition [1,8]. First, carbon can form as a result of reactions over a catalyst. This process has been very well studied over Ni, Fe, and Co, both for catalytic applications [9–16] and for "dusting", also known as "dry corrosion", the problem of pitting when steels are exposed to hydrocarbons at high temperatures [17,18]. The mechanism on each of these metals involves deposition of a carbon source onto the metal surface, dissolution of the carbon into the bulk of the metal, and finally precipitation of carbon as a graphite fiber at some surface of the metal particle. It is important to recognize that the metal is not merely covered by carbon in this reaction, but becomes part of the carbon fiber, explaining the pitting that is observed in dry corrosion. The mechanism also explains why it is necessary to use very high H_2O:C ratios for steam reforming of hydrocarbons with larger molecular weight than that of methane on Ni catalysts [6,19]. Filament formation on Ni occurs when carbon deposition onto the Ni surface occurs more rapidly than carbon removal by steam, even if thermodynamic calculations show that carbon should not be stable at equilibrium.

Carbonaceous compounds can also form in the absence of a catalyst via free-radical, gas-phase condensation reactions [20]. These reactions are most important for hydrocarbons larger than methane and are usually initiated by C–C bond scission at high temperatures. While the primary products of pyrolysis are molecules that are smaller than the parent hydrocarbons, the olefins that are formed by pyrolysis can react with radicals to form larger molecules. The carbonaceous products that are ultimately formed by pyrolysis are high-molecular weight, polyaromatic compounds [8,20], perhaps best referred to as tars and quite different in form from the graphitic fibers on Ni, Co, and Fe catalysts. Because C–H bonds are much stronger than C–C bonds, considerably higher temperatures are required to pyrolyze CH_4 compared to larger alkanes. It is also noteworthy that calculations suggest H_2O does not appear to enter into the gas-phase reactions [20], so that the addition of steam provides no obvious gas-phase reaction for preventing carbon formation and establishing equilibrium between carbon deposits and the hydrocarbon.

Our team has been developing SOFC anodes based on Cu, ceria, and yttria-stabilized zirconia (YSZ) for direct utilization of hydrocarbons ranging from methane to light- and heavy-naphtha. Unlike Ni, none of the materials in the Cu-based anodes is a catalyst for carbon formation [1,21–24]. However, because SOFC require high operating temperatures, tars are formed on the anode by gas-phase pyrolysis [8]. In principle, it should be possible to use the steam generated within the anode by oxidation of the hydrocarbon to oxidize these tars; but the conditions under which this will occur are not established.

In this study, we will describe experiments aimed at characterizing carbon deposition in direct-utilization SOFC anodes utilizing liquid hydrocarbon feeds and the removal of these carbon deposits using steam. We will show that the reaction of carbon with steam depends strongly on the composition of the surface on which carbon is formed, so that carbon can be controlled at reasonable H_2O:C ratios when a catalytic surface is present.

2. Experimental techniques

The fuel-cell tests in this study were performed on cells having a Cu (30 wt.%)–ceria (10 wt.%)–YSZ anode, a 60 μm electrolyte, and a conventional LSM–YSZ cathode. These cells were essentially identical to those used in previous studies [24]. The anodes were prepared by impregnation, using the nitrate salts of Cu and Ce, of the porous side of a porous-dense YSZ bilayer, prepared by tape-casting with pore formers. Electrical contact with the cells was achieved using Ag paste and a Ag wire at the cathode and a Au wire with Au paste at the anode. The cells were then attached to an alumina tube using a ceramic adhesive (Aremco, Ceramabond 552). All impedance spectra were measured in the galvanostatic mode with a frequency range from 0.01 Hz to 100 kHz and a 1 mA ac perturbation, using a Gamry Instruments Potentiostat, as described elsewhere [25].

In humidified (3% H_2O) H_2 at 973 K, these cells all exhibited linear *V–i* polarization curves, an open-circuit voltage (OCV) of 1.1 V, and a maximum power density between 220 and 240 mW cm^{-2}, depending on the cell. In this paper, we will focus on the data for hydrocarbon fuels. Liquid fuels were fed to the cells with a syringe pump at 2 ml h^{-1}, without dilution [26]. Because the active area of the fuel cells was only 0.36 cm^2, the fuel utilizations in all of the experiments described here were less than 2% [27].

For the experiments with undiluted hydrocarbons as fuel, we observed that the deactivation of cells depended on the length of the pre-heat zone for the fuels entering the anode chamber. Cells deactivated much more rapidly when this preheat zone was long, a result that provided an early indication that gas-phase reactions were responsible for tar formation. (Note: we have previously established that the carbon deposited by gas-phase pyrolysis is a mixture of polyaromatic compounds having very low vapor pressures [8]. In this paper, we will refer to these compounds as "carbon" or tar.) To minimize these gas-phase reactions, the tubes on which the cells were attached were placed only 3 cm into the furnace in order to minimize the pre-heat zone. The cell temperature was not affected by this cell placement,

as demonstrated by the fact that the initial *V–i* polarization curves and the ohmic resistances (associated with the electrolyte) in the impedance spectra were unaffected by the placement of the cells or the length of the pre-heat zone [24].

The measurements used to quantify carbon deposition and removal were performed on YSZ slabs, approximately 2 mm × 2 mm × 10 mm, that were made from the same slurries used to tape cast the anode layers in the fuels cells. These slurries included graphite and polystyrene pore formers, so that the slabs had a porosity of 65% after having been fired to 1823 K. The slabs had a bimodal pore-size distribution, with 1.5 μm pores arising from the graphite pore formers and 20 μm pores from the polystyrene [28]. The BET surface area of the slabs was 0.7 $m^2\,g^{-1}$ [29]. Ceria and/or Cu was added to some of the slabs using aqueous solutions of $Ce(NO_3)_3$ and $Cu(NO_3)_2$. To estimate tar formation rates, the slabs were exposed to different fuels at various temperatures for 4 h in a quartz tubular reactor, having a 0.4 cm inside diameter. The results depended on the hydrocarbon flow rates. These are reported as residence times for the hydrocarbons within the hot-zone of the reactor, calculated assuming no reaction and ideal gas law behavior. After hydrocarbon exposures, the tubes were flushed with He for 1 h at the exposure temperature, then removed from the reactor and weighed.

The reactivity of deposited carbon with steam was measured on the same slabs using Temperature programmed oxidation (TPO), with steam as the oxidant. Using a similar, quartz-tube reactor, the samples were exposed to 20 vol.% H_2O in He, with a He flow rate of 30 ml min^{-1}. A syringe pump was used to add distilled water directly to the reactor, and the heating rate in these experiments was 2 K min^{-1}. An ice bath was used to trap the majority of the water at the reactor exit, allowing the composition of the remaining gases to be sampled with a residual-gas analyzer.

To demonstrate that carbon deposition and removal could occur simultaneously, we exposed the ceria-containing YSZ slabs from the TPO experiments to mixtures of H_2O and *n*-butane at 973 K. After flushing the system with He, any remaining carbon on the sample was oxidized using 20% H_2O in He at 973 K. The presence of carbon in these experiments was detected by the H_2, CO, and CO_2 that was produced.

A number of different fuels were used in this study. In addition to the pure-compound fuels, *n*-butane, *n*-decane, and toluene, we also examined the stability of our cells using proprietary petroleum-based liquid hydrocarbon fuels produced by Saudi Aramco. These light and a heavy naphtha range fuels were produced in a commercial 350,000 BPD refinery and processed using specialized fuel processing methods in a custom built 500 $cm^3\,h^{-1}$ pilot plant [30,31]. The candidate fuels produced in Saudi Aramco were analyzed and cross analyzed for typical properties using standard ASTM methods, with some of those properties listed in Table 1. These fuels vary in boiling point distribution, density, viscosity, lower heating value, and aromatics, paraffins, carbon, and hydrogen content.

Table 1
Fuel sample properties

Properties	Light naphtha	Heavy naphtha
Specific gravity	0.659	0.714
API gravity, 60 °F	83.9	64.3
Sulfur (ppm)	<1	<1
Nitrogen (ppm)	<1	<1
Hydrogen (wt.%)	16.17	15.31
Carbon (wt.%)	83.83	84.69
Mol weight (g mol^{-1})	81.0	107.5
Research octane (RON)	61.5	48.8
Heating value (Btu lb^{-1})	19,500	20,000
PIONA (wt.%)[a]		
Paraffins	51.9	32.1
Isoparaffins	39.8	35.8
Olefins	0.00	0.00
Naphthenes	6.44	29.9
Aromatics	1.88	1.09
Unidentified	0.00	1.31
SIMDIS (°F)[b]		
5%	98	152
10%	99	166
20%	129	190
30%	131	200
40%	133	222
50%	141	238
60%	151	252
70%	153	279
80%	154	295
90%	156	333
95%	167	358
FBP	202	398

[a] Parrafins, iso-paraffins, olefins, naphthenes and aromatics (PIONA) analyzes a fuel sample using gas chromatography, comparing the peaks with established standards in the gasoline boiling range, as described under ASTM # D-5134-98.

[b] Simulated distillation (SIMDIS) measures the boiling-point distribution according to ASTM method # D-2887-04A.

3. Results

3.1. Fuel-cell tests

Fig. 1a shows the *V–i* polarization curves for a cell operating on *n*-decane at 973, 1023, and 1073 K. As discussed in the Section 2, the undiluted fuel was injected directly into the fuel-cell anode compartment with a syringe pump, through a quartz capillary tube. Vaporization of the fuel occurred in the quartz capillary as it extended into the furnace. The *V–i* curves for *n*-decane are essentially identical to what we observed with *n*-butane in similar cells [22]. Unlike the case for H_2 (Fig. 1b), the *V–i* curves with hydrocarbon fuels are highly curved at lower voltages, with a shape that suggests reaction of the hydrocarbons is polarization activated [32]. Furthermore, the OCV for the hydrocarbons, approximately 1.0 V for *n*-decane in this temperature range, is lower than the predicted Nernst potentials [33]. The maximum power densities in *n*-decane were 100, 170, and 240 mW cm^{-2}, respectively, at 973, 1023, and 1073 K. Notice that higher power densities can be achieved through the use of thin electrolytes and

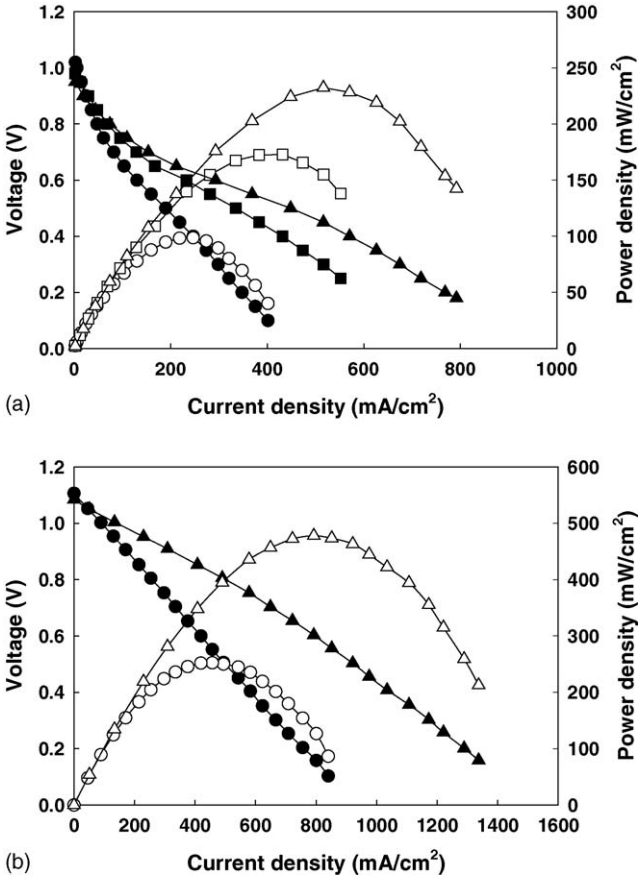

Fig. 1. (a) Cell potentials (solid symbols) and power densities (open symbols) as a function of current density for cells operating on undiluted *n*-decane at 973 K (–●–), 1023 K (–■–) and 1073 K (–▲–). (b) Cell potentials (solid symbols) and power densities (open symbols) as a function of current density for cells operating on humidified (3% H_2O) H_2 at 973 K (–●–) and 1073 K (–▲–).

better cathodes but this was not the primary focus of our study.

Fig. 2 shows the power densities at 0.5 V for pure, undiluted *n*-decane as a function of time at 973, 1023, and 1073 K.

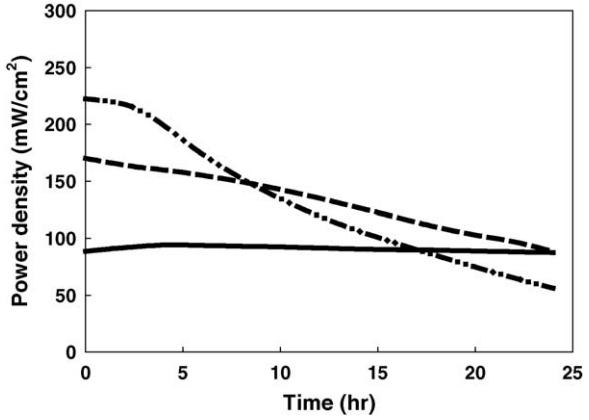

Fig. 2. Power densities at 0.5 V as a function of time for *n*-decane at 973 K (—), 1023 K (– – –), and 1073 K (–···–).

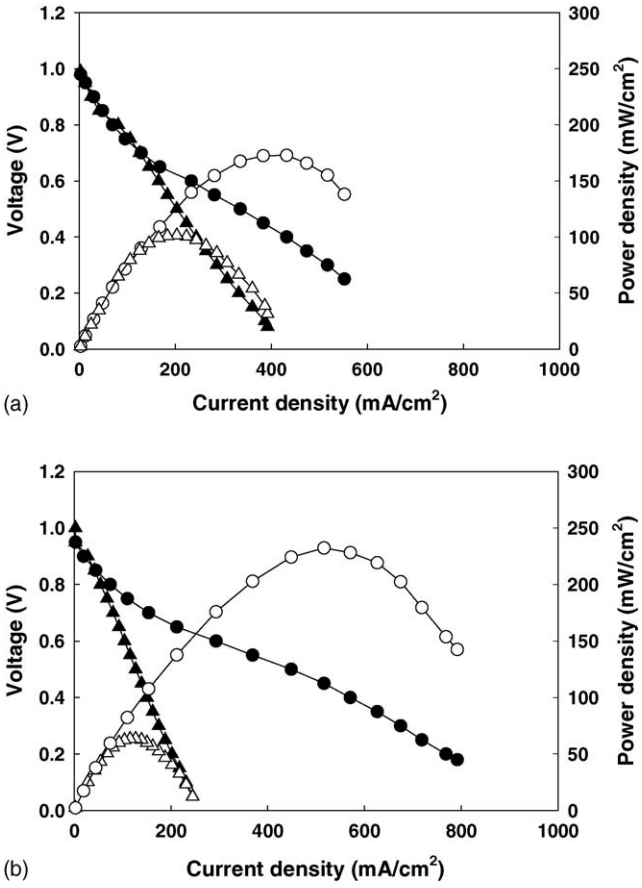

Fig. 3. (a) Cell potentials (solid symbols) and power densities (open symbols) as a function of current density for cells operating on undiluted *n*-decane at 1023 K. The data show the initial performance (–●–) and the performance after 24 h operation (–▲–). (b) Cell potentials (solid symbols) and power densities (open symbols) as a function of current density for cells operating on undiluted *n*-decane at 1073 K. The data show the initial performance (–●–) and the performance after 24 h operation (–▲–).

For a period of 24 h, the power density at 973 K is reasonably stable. However, at 1023 K, the power density dropped from 170 to 100 mW cm^{-2}; in this time period at 1073 K, the power density dropped from 230 to 60 mW cm^{-2}. We suggest that the deactivation observed in Fig. 2 is likely associated with the anode pores being filled with tar-like molecules. First, the cell performance after 24 h in *n*-decane at 1023 and 1073 K could be restored to near its initial value by oxidation in lab air for 10 min. The oxidation step would be expected to remove tars from the pores but should not otherwise reactivate the cell. Second, the *V–i* polarization curves are consistent with diffusion limitations in the deactivated cells. Fig. 3a shows the *V–i* plots for the cell at 1023 K at the beginning and end of a 24 h run. Assuming that the anode pores are largely filled with carbon at the end of the test period, diffusion, either of the fuel to the three-phase boundary or of water and CO_2 from the three-phase boundary, would limit the performance most at higher current densities, exactly where the changes

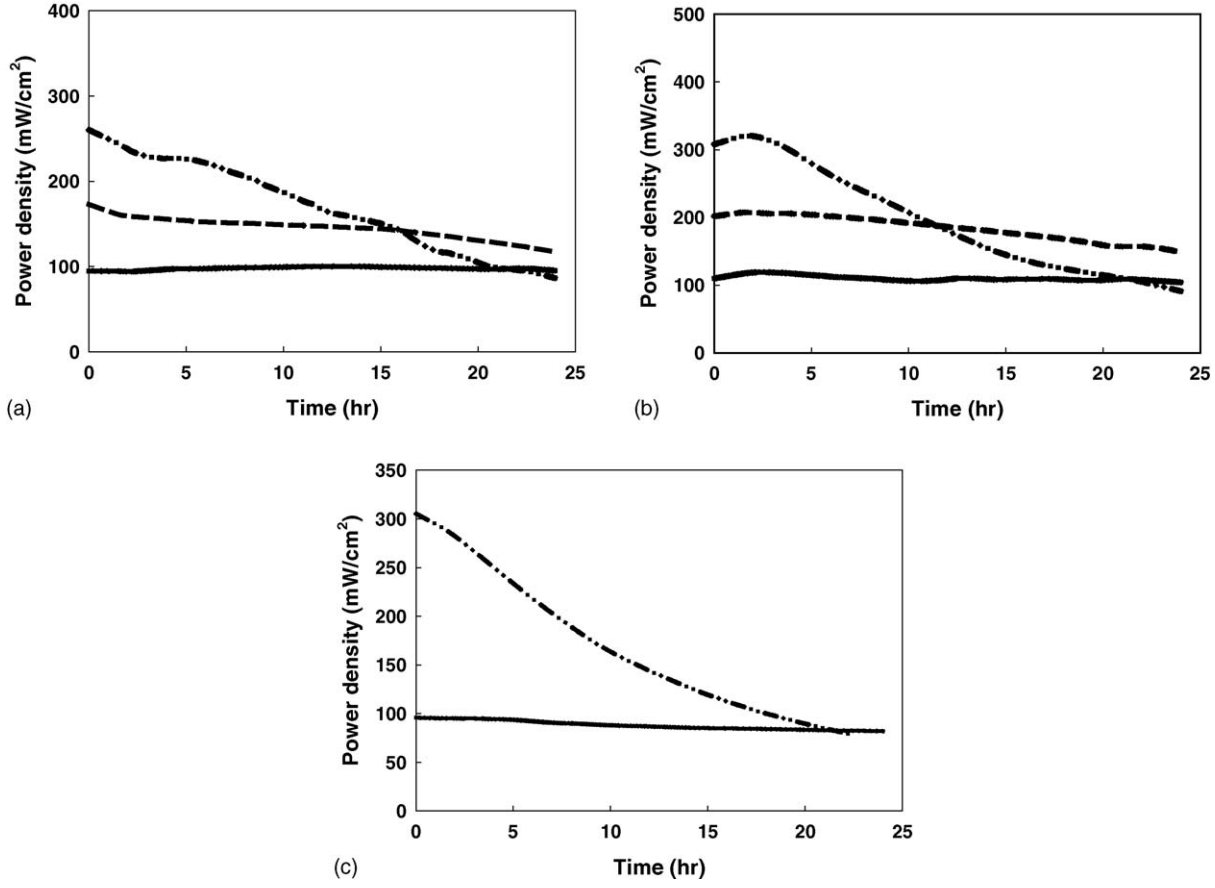

Fig. 4. Power densities at 0.5 V as a function of time for a cell operating on (a) the light naphtha, (b) the heavy naphtha and (c) the mixture of 20 vol.% toluene and 80 vol.% *n*-decane. The operating temperatures were 973 K (—), 1023 K (– – –), and 1073 K (–··–).

in the *V–i* curves occur. The results at 1073 K, Fig. 3b, were more severe but showed the same trend.

Carbon formation on Ni catalysts depends strongly on the nature of the hydrocarbon [6]; however, on the Cu–ceria–YSZ anodes, the results for various hydrocarbons other than methane were very similar. For example, the stability data when using *n*-butane as the fuel were virtually identical to the results shown in Fig. 2 for *n*-decane. An additional demonstration of the similarity of deactivation with different fuels is given in Fig. 4, which shows the performance as a function of time at various temperatures using the light naphtha, the heavy naphtha, and a fuel mixture of 80 vol.% *n*-decane and 20 vol.% toluene. Each of these fuels has different hydrocarbon distributions and the latter mixture has a relatively large concentration of toluene which is a potential precursor to the polyaromatic tars that form upon deactivation [8]. Fig. 4 shows that the deactivation rates for each of these fuels was essentially identical to that of *n*-decane, indicating that the polyaromatics are formed irrespective of aromatic content in the precursor fuel. At 973 K, the performance was reasonably stable for the 24 h period, while deactivation at 1073 K was severe. The approximate rate of deactivation at 1073 K appeared to be essentially identical for each of the fuels.

3.2. Carbon deposition rates

To gain information on the amounts of carbon that form in the anode and the temperature range where this formation becomes important, we measured the weight change of a YSZ slab exposed to *n*-butane for 4 h in our quartz-tube reactor, with the results shown in Fig. 5. The results for experiments performed with *n*-decane were again similar, however, the low vapor pressure of *n*-decane caused condensation at the reactor exit that made it more difficult to remove the samples for measurement of the weights.

From the data in Fig. 5, it can be seen that there is a temperature threshold at approximately 950 K, above which significant amounts of carbon begin to form. This is almost identical to what has been reported previously for tar formation by gas-phase pyrolysis of *n*-butane by Sheng and Dean [20]. Furthermore, with 100% *n*-butane being fed to the reactor, the amount of carbon that deposited on the slab depended on the residence time of *n*-butane in the reactor. More carbon formed with longer residence times, corresponding to lower flow rates. For homogeneous reactions, an increased residence time should give higher conversions, so that this result is again consistent with carbon deposition occurring by a gas-phase homogeneous reaction.

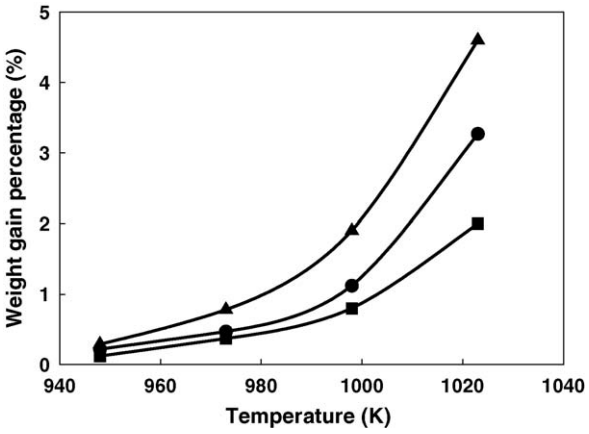

Fig. 5. The weight gain for a 65% porous, YSZ slab following 4 h exposures to *n*-butane at different temperatures. The data are shown for undiluted *n*-butane with residence times of 9 s (–▲–) and 3 s (–●–). Data are also shown for *n*-butane diluted in steam (–■–). For these experiments, the *n*-butane residence time was approximately 3 s and the H_2O:C ratio was fixed at 1.5.

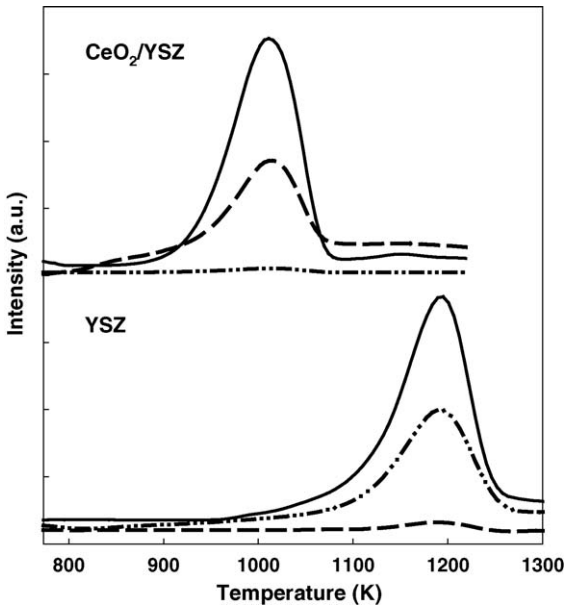

Fig. 6. TPO results, using 20 vol.% H_2O in He as the oxidant, for ceria–YSZ and YSZ slabs exposed to *n*-butane at 973 K for 2 h. The monitored products were: —, H_2 (*m*/*e* = 2); – – –, CO_2 (*m*/*e* = 44), and –·–, CO (*m*/*e* = 28).

In what is perhaps the most interesting result from Fig. 5, we observed tar formation even when the *n*-butane was fed together with steam at a H_2O:C ratio of 1.5. The amount of carbon that formed in the presence of steam was somewhat less than that which formed in pure *n*-butane, but this result can be explained completely by the fact that gas-phase concentration of *n*-butane was significantly lower due to the presence of steam. It is noteworthy that carbon is not thermodynamically stable for a H_2O:C ratio of 1.5 in this temperature range; therefore, the fact that carbon formed in this experiment is further proof that thermodynamic calculations cannot be used to predict carbon formation in this configuration.

Comparing the results in Fig. 5 to the deactivation data from the previous section tends to confirm our earlier point that a significant fraction of the anode pores are likely filled with carbon in the deactivated cells. Assuming that the density of the carbon deposits is similar to that of a polyaromatic molecule, such as anthracene, 1.28 g cm^{-3}; 5 wt.% carbon corresponds to filling of approximately 12% of the pore volume within the YSZ slab. After 24 h and 1073 K, one would expect the pores to be essentially completely filled with carbon, explaining the severe deactivation.

Finally, we measured carbon-deposition rates on YSZ slabs containing 10 wt.% ceria and 20 wt.% Cu. Within experimental error, the results were found to be indistinguishable from that found in Fig. 5. This is again consistent with the carbon deposits forming in the gas phase, with the solid simply providing a surface onto which the deposits condense.

3.3. Carbon removal by steam

Carbon formation by free-radical, gas-phase reactions is probably unavoidable for most hydrocarbon fuels other than methane in the temperature range between 973 and 1073 K. However, if the rate of carbon removal is fast compared to the rate of carbon deposition, it should be possible to operate the system at steady state. To understand the oxidation of carbonaceous deposits by steam, we first performed TPO measurements, using 20 vol.% H_2O in He as the oxidant, on YSZ slabs, one with 15 wt.% ceria and one without. For the results shown in this paper, carbon was deposited by exposing the samples to *n*-butane at 973 K for 2 h; however, results obtained by exposing the samples to *n*-decane were essentially identical. For *n*-butane exposure on the ceria–YSZ and YSZ slabs, the weight change indicated 5 mg of carbon per gram of sample were deposited and all of this carbon was removed at the end of the TPO measurement. The TPO results are shown in Fig. 6.

With pure YSZ, there is no evidence for reaction below approximately 1023 K and most of the carbon is oxidized between 1073 and 1273 K. Furthermore, the main carbon-containing product in the TPO with steam is CO, with only negligible amounts of CO_2 being formed, even though equilibrium considerations would suggest that CO_2 should be the preferred product. Based on the fact that carbonaceous deposits on the walls of the quartz reactor were oxidized in exactly this same temperature range and that CO was the preferred product in that case as well, we conclude that the YSZ has no effect in this reaction. Furthermore, since carbon deposition was performed at 973 K and carbon removal is negligible below 1023 K, the TPO result implies that the removal of carbon will occur much more slowly than the rate of deposition in this temperature range. This is consistent with the fact that the addition of steam together with *n*-butane in the data shown in Fig. 5 had little effect on carbon deposition other than to dilute the hydrocarbon.

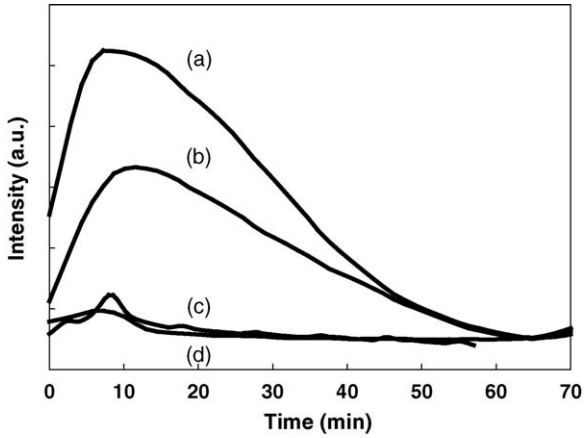

Fig. 7. Examples of data obtained for carbon removal from a YSZ slab containing 15 wt.% ceria by 20 vol.% H_2O in He at 973 K. The data shows the evolution of H_2 due to reaction of carbon with H_2O. Prior to steam exposure, the sample was exposed to *n*-butane for 2 h, using an *n*-butane residence time of 3 s and various H_2O:C ratios, then flushed with He for 1 h. The following H_2O:C ratios were used during *n*-butane exposure: (a) 0.2, (b) 0.3, (c) 0.4, and (d) 0.5.

Upon the addition of ceria to the YSZ slab, the reaction temperature required to oxidize carbon shifted downward, indicating that ceria actively catalyzes the removal of carbon. Reaction became significant at 923 K and all of the carbon was removed below 1073 K. Also, the main carbon-containing product in the TPO was CO_2, indicating that the presence of ceria promotes the high-temperature water–gas-shift reaction. While ceria had a negligible impact on carbon deposition, the TPO indicate that it promotes the removal of carbon by steam.

To determine whether carbon formation and removal can occur simultaneously over ceria–YSZ slabs in the presence of H_2O and *n*-butane, we exposed samples with 15 wt.% ceria to various *n*-butane–H_2O mixtures at 973 K for 2 h. Following exposure, the presence of carbon on the slabs was detected by flowing a 20% H_2O–He mixture over the slabs at 973 K, using the production of H_2, CO, and CO_2 in the reactor effluent to determine the relative amount of carbon. That steam at 973 K was sufficient to completely remove all carbon from the ceria-containing samples was checked by weighing the slabs at the end of some of the experiments and demonstrating that their weights returned to the initial values.

Fig. 7 shows examples of the raw data for H_2 production obtained upon exposing a slab to the H_2O–He mixture, after it had been exposed to mixtures of *n*-butane and H_2O at 973 K. In each case, the production of H_2 was matched by the production of CO_2 and CO, so that H_2 production is an indication that carbon had been present on the sample. For this set of experiments, the *n*-butane residence time in the reactor was maintained at 3 s. What the results show is that no carbon formed when the H_2O:C ratio was greater than 0.4. For these conditions, steam removed the carbon faster than it was deposited by the gas-phase pyrolysis reaction. Experiments on a YSZ slab containing 20 wt.% Cu and 10 wt.% ceria were essentially indistinguishable from that shown in Fig. 7, showing that Cu did not block the oxidation of carbon.

As the results in Fig. 5 indicate, the residence time and reaction temperature for *n*-butane are important in the carbon deposition reaction. Holding the H_2O:C ratio at 0.5 at 973 K, we did not observe carbon formation after 2 h for residence times of 3, 5 and 7 s; however, carbon formation was observed for residence times greater than 9 s at this H_2O:C ratio. Likewise, for a H_2O:C ratio of 0.5 and a residence time of 7 s, carbon did not form at 973 or 1023 K but carbon was observed for these conditions at 1073 K.

4. Discussion

Carbon formation in high-temperature processes involving hydrocarbons can be a severe problem. Based on the results of this study, a number of important lessons can be drawn concerning the issue, the most important being that understanding the mechanisms of carbon formation can be crucial in developing strategies to avoid the problem. Thermodynamic calculations do not provide good predictions due to the fact that the formation and removal rates for carbon can be relatively slow. Furthermore, changing the composition of the surfaces onto which the carbon deposits can dramatically change the rates. In the case of ceria, only the rate of carbon removal appears to have been affected, since, in the absence of steam, we observed no difference in the deposition rates for *n*-butane between YSZ and YSZ with ceria. Similarly, metals like Ni, Fe, and Co participate actively in carbon formation while Cu does not.

In SOFC applications, the mechanism for carbon formation is also important for understanding the nature of deposits and how these will affect the cell. For example, carbon formation on Ni-based anodes involves more than simply covering the electrode. The formation of carbon fibers can result in Ni removal from the electrode (dusting); even more important, significant pressures can arise within the electrode as the fibers grow, causing the electrode to fracture [34]. By contrast, carbon deposition on the Cu-based anodes in this study deactivates the cell by filling the pores without causing physical damage. It was even demonstrated that the cell performance could be at least partially restored by removing the carbon through oxidation, with the slight deactivation that we observed upon removing the carbon likely associated with oxidizing the anode. If oxidation had been performed in a more controlled manner with steam, cell performance might not have been affected.

The fact that carbon formation with the Cu-based electrodes is associated with gas-phase, free-radical reactions suggests strategies for avoiding carbon formation even with heavier liquid hydrocarbons. Obviously, if one can work at low temperatures, below the threshold where pyrolysis occurs, carbon formation should be avoided. Minimizing the free volume within the anode will also significantly decrease

the amount of carbon that forms by decreasing the residence time of the fuel. In addition, it may be possible to affect the free-radical reactions through fuel additives or through surfaces in the anode compartment that might terminate the radicals before polymerization to high-molecular weight products has occurred. Modification of the initiation or termination steps in free-radical reactions are well known in combustion reactions and may well be possible in this application as well.

The other means of controlling carbon in Cu-based anodes is through the use of ceria coatings that would allow carbon to be removed by reaction with steam as fast as the carbon forms. Steam will be present in the anode under realistic conditions since significant amounts of steam will be generated by oxidation of the hydrocarbon fuels. For example, the H_2O:C ratio for *n*-butane at 50% fuel utilization will be 1.2. One would also expect the rate of carbon oxidation by steam to depend on the catalytic surface area. This would suggest that packing the free volume within the anode with a high-surface area, ceria-based catalyst may well increase the rate of carbon consumption and so stabilize the cells to even lower H_2O:C ratios than we observed in our study. Because the gas-phase pyrolysis reactions are very well understood [20], it should be possible to develop accurate models to determine when and where carbon might form.

Clearly, carbon formation is an issue for SOFC that oxidize hydrocarbons directly. In this paper, we have demonstrated that a fundamental understanding of the mechanisms of carbon deposition and removal can lead to strategies to minimize the problem.

5. Conclusions

Gas-phase, free-radical reactions can lead to the formation of high-molecular weight polyaromatic compounds in the anodes of SOFC that operate directly on hydrocarbon fuels, even when using anodes that do not catalyze the formation of carbon. These compounds deactivate the anode by essentially filling the pores. However, it is possible to oxidize these polyaromatic compounds using steam generated in the electrochemical reactions if the surface of the anodes contains catalytically active compounds, such as ceria. In this paper, we have outlined strategies that can be used to avoid carbon formation.

Acknowledgement

This work was funded by a grant from the Saudi Arabian Oil Company (Saudi Aramco), with additional assistance from the Office of Naval Research.

References

[1] S. McIntosh, R.J. Gorte, Chem. Rev. 104 (2004) 4845–4865.
[2] T. Takeguchi, Y. Kani, T. Yano, R. Kikuchi, K. Eguchi, K. Tsujimoto, Y. Uchida, A. Ueno, K. Omoshiki, M. Aizawa, J. Power Sources 112 (2002) 588.
[3] K. Eguchi, H. Kojo, T. Takeguchi, R. Kikuchi, K. Sasaki, Solid State Ionics 152/153 (2002) 411.
[4] K. Sasaki, Y. Teraoka, J. Electrochem. Soc. 150 (2003) A878.
[5] K. Sasaki, Y. Teraoka, J. Electrochem. Soc. 150 (2003) A885.
[6] T. Sperle, D. Chen, R. Lødeng, A. Holmen, Appl. Catal. A 282 (2005) 195.
[7] Y. Zhang, K.J. Smith, Catal. Lett. 95 (2004) 7.
[8] S. McIntosh, H. He, S.-I. Lee, O. Costa-Nunes, V.V. Krishnan, J.M. Vohs, R.J. Gorte, J. Electrochem. Soc. 151 (2004) A604–A608.
[9] R.T.K. Baker, M.A. Barber, P.S. Harris, F.D. Feates, R.J. Waite, J. Catal. 26 (1972) 51.
[10] R.T.K. Baker, P.S. Harris, J. Henderson, R.B. Thomas, Carbon 13 (1975) 17.
[11] R.T.K. Baker, P.S. Harris, S. Terry, Nature 253 (1975) 37.
[12] C.W. Keep, R.T.K. Baker, J.A. France, J. Catal. 47 (1977) 232.
[13] C.H. Bartholomew, Catal. Rev. Sci. Eng. 24 (1982) 67.
[14] R.T.K. Baker, Carbon 27 (1989) 315.
[15] T. Zhang, M.D. Amiridis, Appl. Catal. A 167 (1998) 161.
[16] B. Monnerat, L. Kiwi-Minsker, A. Renken, Chem. Eng. Sci. 56 (2001) 633.
[17] C.M. Chun, J.D. Mumford, T.A. Ramanarayanan, SOFC VI, in: S.C. Singhal, M. Dokiya (Eds.), Proceedings of the Electrochemical Society Series PV 1999-19, The Electrochemical Society, Pennington, NJ, 1999, p. 621.
[18] C.H. Toh, P.R. Munroe, D.J. Young, K. Foger, Mater. High Temp. 20 (2003) 129.
[19] X. Wang, R.J. Gorte, Catal. Lett. 73 (2001) 15.
[20] C.Y. Sheng, A.M. Dean, J. Phys. Chem. A 108 (2004) 3772.
[21] S. Park, J.M. Vohs, R.J. Gorte, Nature 404 (2000) 265.
[22] R.J. Gorte, S. Park, J.M. Vohs, C. Wang, Adv. Mater. 12 (2000) 1465.
[23] R.J. Gorte, J.M. Vohs, J. Catal. 216 (2003) 477–486.
[24] H. He, J.M. Vohs, R.J. Gorte, J. Electrochem. Soc. 150 (2003) A1470–A1475.
[25] S. McIntosh, J.M. Vohs, R.J. Gorte, J. Electrochem. Soc. 150 (2003) A1305.
[26] H. Kim, S. Park, J.M. Vohs, R.J. Gorte, J. Electrochem. Soc. 148 (2001) A693–A695.
[27] O. Costas-Nunes, J.M. Vohs, R.J. Gorte, J. Electrochem. Soc. 150 (2003) A858–A863.
[28] M. Boaro, J.M. Vohs, R.J. Gorte, J. Am. Ceram. Soc. 86 (2003) 395–400.
[29] Y. Huang, J.M. Vohs, R.J. Gorte, J. Electrochem. Soc., in press.
[30] B.O. Dabbousi, A.H. Al-Khawajah, G.D. Martinie, J.C. Cross, A.R. Khan, Proceedings of the 16th World Petroleum Congress, Calgary, AB, Canada, June, 2000.
[31] B.O. Dabbousi, A.H. Al-Khawajah, G.D. Martinie, US Patent Application Publication No. US 2003/0003331 A1, Published January 2, 2003.
[32] J.H. Hirschenhofer, D.B. Stauffer, R.R. Engleman, Fuel Cells: A Handbook, Revision 3, US-DOE/METC-94/1006, Morgantown, WV, 1994, pp. 2–7.
[33] S. McIntosh, J.M. Vohs, R.J. Gorte, Electrochem. Solid State Lett. 6 (2003) A240–A243.
[34] H. Kim, C. Lu, W.L. Worrell, J.M. Vohs, R.J. Gorte, J. Electrochem. Soc. 149 (2002) A247–A250.